IEEE Access
Multidisciplinary | Rapid Review | Open Access Journal

Received April 8, 2022, accepted May 5, 2022, date of publication May 13, 2022, date of current version June 3, 2022.

Digital Object Identifier 10.1109/ACCESS.2022.3174967

Anti-Error Robust Pattern Synthesis Algorithm in Time-Modulated Array Antenna

YUANJIN TIAN, JING TAN, YANWEI ZHANG, KE WANG, XIAO DONG, AND HAILIN LI

Key Laboratory of Radar Imaging and Microwave Photonics, College of Electronic and Information Engineering, Nanjing University of Aeronautics and Astronautics, Nanjing 210016, China

Corresponding author: Yuanjin Tian (nuaatyj@nuaa.edu.cn)

This work was supported by the National Natural Science Foundation of China under Grant 61671239.

ABSTRACT Compared with the traditional antenna array, the time-modulated array can increase the flexibility of the array by adding time switches. However, due to the introduction of time switches, the time-modulated array antenna is more sensitive to random errors than the traditional array. Besides random errors caused by unavoidable factors such as array deformation and defects of processing and assembly in the traditional array, time-modulation parameter errors will be introduced by time switches. As errors in the traditional array can degrade the performance of the array, time-modulation parameter errors can lower the performance of the array pattern as well, which will lift the side-lobe and increase the dynamic range of the side-lobe. Aiming at the time-modulation parameter errors in the time-modulated array, an anti-error robust pattern synthesis algorithm (AERPS) based on the convex optimization (CVX) is proposed in this paper. In the algorithm, the optimization model for the pattern synthesis of the time-modulated array is established and analyzed. Then the model is divided into two sub-models of the center frequency and the first sideband, and the convex optimization solution is first performed on the center frequency model. After the center frequency model is solved, the convex optimization solution is used to solve the first-order sideband model to obtain the final results. The simulation results of the time-modulated array in this paper show that the algorithm can reduce the average value and the dynamic range of the normalized side-lobe level, thus verifying the effectiveness and the robustness of the algorithm.

INDEX TERMS Array antenna, convex optimization, error analysis, pattern synthesis, time-modulated array.

I. INTRODUCTION

Array antenna can achieve higher performance than a single antenna by combining signals with each other. However, due to the manufacturing mistakes and other unavoidable factors, array antenna will be affected by various kinds of errors, such as the position error of elements, the amplitude and phase excitation error, the interval error of elements, etc. These errors will raise the side-lobe of the pattern of arrays, resulting in degradation of the radiation pattern performance. In order to reduce the negative impact of errors, it is necessary to make analysis of errors.

Many researchers have studied the amplitude and phase excitation error in array antenna. Appasani *et al.* proposed a pseudo measurement technique for detection and correction of excitation error of the array antenna [1]. Zahedi and Arand proposed a phase compensation method based on the genetic algorithm to realize the phase error correction for large phased array antennas [2]. Huang *et al.* proposed a non-iterative technique for the self-calibration of the amplitude and phase error of the sensors of the airborne array antenna with unknown source location [3]. Aiming at the amplitude and phase error of the microwave feed network of the phased array radar, Xie *et al.* proposed an array monitoring method based on the compensation and correction technology [4]. Zhang *et al.* proposed an improved calibration method using coefficient matrix for the amplitude and phase error in the phased array radar [5]. Dai *et al.* proposed a new method that does not require a priori calibration information for the problem of amplitude and phase error calibration for large-scale planar arrays [6]. Wang *et al.* proposed a calibration method for circular array antennas with mutual coupling and amplitude and phase error, and obtained a more accurate DOA (Direction of Arrival) estimate [7]. Rocca *et al.* proposed a statistical method based on the interval analysis to analyze the influence of the amplitude and phase excitation

The associate editor coordinating the review of this manuscript and approving it for publication was Hisao Ishibuchi.

with random errors on the radiation pattern of the phased array [8]. He *et al.* introduced how to use the probability-based method and method based on the interval arithmetic to evaluate the effects of the phased array antenna with excitation errors [9].

There are also many literatures that have analyzed and studied the position error of array elements. For the array antenna with element position errors, Lou *et al.* considered the mutual coupling effect in the traditional compensation method to reduce the influence of the array deformation [10]. Yoo *et al.* studied the phased array radar where the antenna feed position is not in the center of the antenna, and proposed a compensation technique that does not collect information at the center of the antenna [11]. Ye *et al.* proposed an equivalent method for estimating signal parameters based on the single-signal source rotational invariance technique, which can effectively balance the position error caused by the vibration deformation of the array [12]. Sippel *et al.* analyzed the antenna array with mutual coupling, unknown time delay and position errors, and proposed a calibration method using an incoherently transmitting beacon [13]. Wang *et al.* proposed the coupled structure-electromagnetic statistic model for the randomness of the position of elements in the antenna array, which can quickly and effectively obtain the antenna performance [14]. Sa *et al.* proposed a hybrid tolerance design method for antenna array with geometric errors, which improved the performance of the antenna [15]. Wang *et al.* proposed a prior knowledge-based algorithm for large array antennas with interval errors, phase excitation errors and position errors, which improved the robustness of the antenna array [16]. Zhang *et al.* analyzed the position error existing in the conformal array and proposed a position error calibration algorithm to reduce the influence of the error [17].

In addition to the excitation error and position error mentioned above, other kinds of errors (including interval error, beam pointing error, etc.) have also been studied in related literature. Zhou *et al.* analyzed the joint array antenna with the array pointing error, and found the error will increase the side-lobe of the array pattern and reduce the gain [18]. Frid *et al.* analyzed installation errors such as platform reflection, diffraction from metal edges, and reflection and refraction in the radome, and proposed a post-processing method to improve DOA estimation accuracy [19]. Guo *et al.* studied large-scale array antennas containing assembly errors. They established an accurate gain prediction model based on the improved extreme gradient boosting algorithm and transfer learning method, and proposed a compensation method to control the error [20]. Aiming at the beam pointing error of phased arrays, Zhang *et al.* proposed a sequential phase feeding algorithm with the minimum beam pointing error for centrally symmetric planar array antennas, and deduced the theoretical expression of the beam pointing error caused by phase quantization errors [21]. Lee and Song conducted a detailed mathematical analysis of the array antennas with the quantization error and interval error, and theoretically

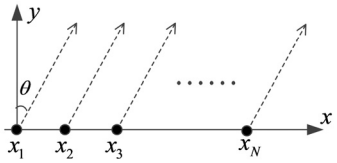

FIGURE 1. Time-modulated linear array.

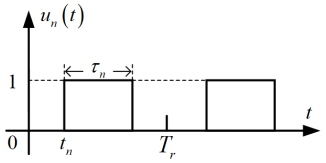

FIGURE 2. Rectangular time-modulation function.

obtained the statistical characteristics of the radiation pattern, which is in good agreement with the simulation results [22].

Compared with the traditional antenna array, the time-modulated antenna array deploys the time-modulation switches, so it will introduce time-modulation parameter errors. These errors in time-modulated arrays have also been studied by some literature. Yurtsev *et al.* analyzed the time interval random errors in the time-modulated array and pointed out that the side-lobe level of the pattern increases faster than that of the array without time-modulation [23]. Amjadian and Fakharzadeh studied the effect of non-ideal time switches on the performance of time-modulated arrays, and pointed out that time error has a little effect on beam pointing and beam width, but more on main-lobe level [24]. However, there is still a lot of room for research on various kinds of errors in time-modulated arrays.

Aiming at the time-modulation parameter errors in the time-modulated array, this paper proposes an anti-error robust pattern synthesis algorithm (AERPS) to optimize time-modulation parameters and the excitation coefficients of array elements, so as to minimize the influence of the errors on the array pattern and further improve the low side-lobe and robust performance. The structure of this paper is as follows: Chapter II introduces the pattern synthesis model of the time-modulated linear array under error conditions. The proposed AERPS algorithm is discussed in detail in Chapter III. Numerical simulation results are presented in Chapter IV to demonstrate the effectiveness and robustness of the proposed algorithm. Finally, conclusions are given in Chapter V.

II. MATHEMATICAL MODEL OF TIME-MODULATED LINEAR ARRAY PATTERN SYNTHESIS UNDER ERROR CONDITIONS

Time-modulated linear array composed of N isotropic array elements is shown in Fig 1 and the far-field radiation intensity can be expressed as

$$E(\theta, t) = \sum_n w_n^* u_n(t)\, e^{jkx_n \sin\theta} e^{j2\pi f_0 t} \tag{1}$$

where f_0, x_n and w_n represent the center frequency of the array, the position and complex excitation coefficient of the $n-th$ element in order. $k = 2\pi f_0/c$ is the carrier propagation coefficient in free space, and c is the speed of light.

As shown in Fig 2, in the time-modulation repetition period T_r, $u_n(t)$ is the rectangular function, and its mathematical expression is

$$u_n(t) = \begin{cases} 1 & t_n \le t \le t_n + \tau_n \\ 0 & others \end{cases} \tag{2}$$

where t_n and τ_n are the opening time and duration time, all satisfying $0 \le t_n, \tau_n \le T_r$. Expanding the Fourier series of the $u_n(t)$, we have

$$u_n(t) = \sum_m a_{nm} e^{j2\pi m f_r t}, m = 0, \pm 1, \ldots \tag{3}$$

where $f_r = 1/T_r$, and a_{nm} is the expansion coefficient, whose expression is

$$a_{nm} = \tau_n f_r \sin c(\pi m \tau_n f_r) e^{-j\pi m f_r (2t_n + \tau_n)} \tag{4}$$

therefore formula (1) can be further expressed as

$$E(\theta, t) = \sum_n \sum_m w_n^* \alpha_n \sin c(\pi m \alpha_n) e^{jkx_n \sin\theta - j\pi m(2\beta_n + \alpha_n)} e^{j2\pi(f_0 + mf_r)t} \tag{5}$$

where $\alpha_n = \tau_n f_r$ and $\beta_n = t_n f_r$ are the normalized duration time and opening time, respectively, satisfying $0 \le \alpha_n, \beta_n \le 1$. The radiation intensity expressions of the array at the center frequency f_0 and the $m-th$ sideband $f_0 + mf_r$ are

$$E_0(\theta, t) = \sum_n w_n^* \alpha_n e^{jkx_n \sin\theta} e^{j2\pi f_0 t} \tag{6}$$

$$E_m(\theta, t) = \sum_n w_n^* \alpha_n sinc(\pi m \alpha_n) \times e^{jkx_n \sin\theta - j\pi m(2\beta_n + \alpha_n)} e^{j2\pi(f_0 + mf_r)t} \tag{7}$$

Ignoring the common factor terms $e^{j2\pi f_0 t}$ and $e^{j2\pi(f_0+mf_r)t}$, the above expressions are rewritten as

$$E_0(\theta) = \sum_n w_n^* \alpha_n e^{jkx_n \sin\theta} \tag{8}$$

$$E_m(\theta) = \sum_n w_n^* \alpha_n sinc(\pi m \alpha_n) e^{jkx_n \sin\theta - j\pi m(2\beta_n + \alpha_n)} \tag{9}$$

Next we will discuss the effect of errors on the radiation intensity. Array errors usually contains the following types: excitation errors of the array elements, position errors of the array elements, and time-modulation parameter errors. Only the time-modulation parameter errors are studied in this paper, that is, the opening time error and duration time error are studied.

Assuming that the time switch of the $n-th$ element has normalized opening time error $\Delta\beta_n$ and normalized duration time error $\Delta\alpha_n$, the modified expression of the array antenna's $m-th$ radiation intensity is

$$\begin{aligned} F_m(\theta) &= \sum_n \left(w_n^* (\alpha_n + \Delta\alpha_n) \operatorname{sinc}[m\pi(\alpha_n + \Delta\alpha_n)] \right. \\ &\quad \left. \times e^{jkx_n \sin\theta - jm\pi(2\beta_n + \alpha_n + 2\Delta\beta_n + \Delta\alpha_n)} \right) \\ &= \sum_n \left\{ \left[w_n^* \alpha_n \operatorname{sinc}(m\pi\alpha_n) e^{-jm\pi(2\beta_n + \alpha_n)} \right] \right. \\ &\quad \times \left\{ \left(1 + \frac{\Delta\alpha_n}{\alpha_n} \right) \cdot \frac{\operatorname{sinc}[m\pi(\alpha_n + \Delta\alpha_n)]}{\operatorname{sinc}(m\pi\alpha_n)} \right. \\ &\quad \left. \left. \times e^{-jm\pi(2\Delta\beta_n + \Delta\alpha_n)} \right\} \times e^{jkx_n \sin\theta} \right\} \end{aligned} \tag{10}$$

The part in {} is the sum of the error terms caused by the time-modulation parameter errors $\Delta\alpha_n$, $\Delta\beta_n$.

For the pattern synthesis of the time-modulated linear array affected by the errors, we have studied the following problems: 1)Beamforming in the given direction at the center frequency f_0. 2)Beamforming with given parameters on the first sideband $f_0 + f_r$. 3)Making the peak side-lobe level (PSLL) as low as possible at the center frequency f_0 and first sideband $f_0 + f_r$.

In summary, the comprehensive optimization model of the pattern synthesis is given below

$$\begin{aligned} &\min_{\alpha, \beta, \mathbf{w}} \varepsilon_1, \varepsilon_2 \\ &s.t.\ F_0(\theta_0) = 1 \\ &\quad F_1(\theta_1) = \mu_1 \\ &\quad F_0(\theta_s) \le \varepsilon_1, \theta_s \in \Omega_s \\ &\quad F_1(\theta_s) \le \varepsilon_2, \theta_s \in \Omega_s \\ &\quad 0 \le \alpha_n, \beta_n \le 1 \end{aligned} \tag{11}$$

In the model, $\boldsymbol{\alpha} = \left[\alpha_1 \cdots \alpha_n \right]^T$, $\boldsymbol{\beta} = \left[\beta_1 \cdots \beta_n \right]^T$ are the time modulation parameter vectors that need to be optimized, and they forms the optimal solution vectors of the optimization problem together with the complex excitation coefficient vector $\mathbf{w} = \left[w_1 \cdots w_n \right]^T$. $F_0(\theta_0)$ represents the radiation intensity in the beam direction θ_0 at the center frequency f_0. $F_1(\theta_1)$ represents the radiation intensity in the beam direction θ_1 at the first sideband $f_0 + f_r$, and μ_1 is its maximum value. $F_0(\theta_s)$ and $F_1(\theta_s)$ represent the radiation intensity of the sampling direction θ_s in the side-lobe area Ω_s at the center frequency and first sideband, respectively, and ε_1, ε_2 are the side-lobe constraint parameters.

III. ANTI-ERROR ROBUST PATTERN SYNTHESIS OF TIME-MODULATED LINEAR ARRAY

The model (11) will be divided into two sub-models of the center frequency f_0 and first sideband $f_0 + f_r$.

At the center frequency $m = 0$, according to (10), we have

$$F_0(\theta) = \sum_n w_n^* (\alpha_n + \Delta\alpha_n) e^{jkx_n \sin\theta} \tag{12}$$

Defining a new parametric variable $\chi_n = w_n^* \alpha_n$ and its vector form $\boldsymbol{\chi} = \left[\chi_1 \cdots \chi_n \right]^T = \mathbf{w}^* \cdot \alpha$ which need to be optimized. Denoting $\mathbf{b}_\theta = \left[e^{jkx_1 \sin\theta} \cdots e^{jkx_N \sin\theta} \right]^T$ as the steering vector at the sampling direction θ. At the same time we define $\mathbf{b}_\Delta = \left[\frac{\Delta\alpha_1}{\alpha_1} e^{jkx_1 \sin\theta} \cdots \frac{\Delta\alpha_N}{\alpha_N} e^{jkx_N \sin\theta} \right]^T$, so we have

$$F_0(\theta) = \chi^T \mathbf{b}_\theta + \chi^T \mathbf{b}_\Delta \tag{13}$$

Assuming X is a random vector, and $\mathcal{E}(X)$, $\mathcal{D}(X)$ are the expectation and variance of X, respectively. Under the assumption of $\Delta\alpha_n \overset{i.i.d.}{\sim} N\left(0, \sigma_1^2\right)$, $\mathbf{b}_\Delta$ is a complex Gaussian random vector and the expectation and variance are $\mathcal{E}(\mathbf{b}_\Delta) = \mathbf{0}_{N\times 1}$ and $\mathcal{D}(\mathbf{b}_\Delta) = \sigma_1^2 \cdot diag\left(\frac{1}{\alpha_1^2} \cdots \frac{1}{\alpha_N^2}\right)$, respectively.

According to (13),the error term in $F_0(\theta)$ is $\chi^T\mathbf{b}_\Delta$,whose statistical average power is

$$P_0(\theta) = \mathcal{E}\left\{\left(\chi^T\mathbf{b}_\Delta\right)\left(\chi^T\mathbf{b}_\Delta\right)^H\right\} = \sigma_1^2\sum_n \frac{|\chi_n|^2}{\alpha_n^2} \quad (14)$$

therefore when the parametric vector χ remains unchanged, increasing α_n can reduce the error power. At the same time, for further analysis, according to the triangle inequality in vector form $|\mathbf{X}|-|\mathbf{Y}| \le |\mathbf{X}+\mathbf{Y}| \le |\mathbf{X}|+|\mathbf{Y}|$ and the Cauchy inequality in vector form $\left|\mathbf{X}^T\mathbf{Y}\right| \le \|\mathbf{X}\|_2\|\mathbf{Y}\|_2$, there is

$$\left|\chi^T\mathbf{b}_\theta\right| - \|\chi\|_2\|\mathbf{b}_\Delta\|_2 \le |F_0(\theta)| \le \left|\chi^T\mathbf{b}_\theta\right| + \|\chi\|_2\|\mathbf{b}_\Delta\|_2 \quad (15)$$

where $\|\mathbf{b}_\Delta\|_2^2 = \mathbf{b}_\Delta^H\mathbf{b}_\Delta = \sum_n\left(\frac{\Delta\alpha_n}{\alpha_n}\right)^2$, $\|\mathbf{b}_\Delta\|_2 = \sqrt{\sum_n\left(\frac{\Delta\alpha_n}{\alpha_n}\right)^2}$.

We further introduce the positive real parameter η which is the upper bound of the error term, and for the random vector $\mathbf{b}_\Delta$, $P\{\|\mathbf{b}_\Delta\|_2 \le \eta\} = 1$ statistically holds. We intend to enhance the robustness of the pattern under the error condition by setting the upper bound η. With (15), we have

$$\left|\chi^T\mathbf{b}_\theta\right| - \eta\|\chi\|_2 \le |F_0(\theta)| \le \left|\chi^T\mathbf{b}_\theta\right| + \eta\|\chi\|_2 \quad (16)$$

The term $\chi^T\mathbf{b}_\theta$ in the above formula is exactly the radiation intensity without error, that is $E_0(\theta)$, therefore the upper/lower bound of the radiation intensity under the error condition is obtained

$$|E_0(\theta)| - \eta\|\chi\|_2 \le |F_0(\theta)| \le |E_0(\theta)| + \eta\|\chi\|_2 \quad (17)$$

because of the equation $\mathcal{E}\left\{\|\mathbf{b}_\Delta\|_2^2\right\} = \sum_n \frac{\mathcal{E}\{(\Delta\alpha_n)^2\}}{\alpha_n^2} = \sigma_1^2\sum_n\frac{1}{\alpha_n^2}$, $\eta \ge \sqrt{\mathcal{E}\left\{\|\mathbf{b}_\Delta\|_2^2\right\}} = \sigma_1\sqrt{\sum_n\frac{1}{\alpha_n^2}}$ can be selected as a typical value. In summary, the anti-error robust pattern synthesis problem at the center frequency can be solved by two steps:

1)Enhance the robustness of the array pattern with the parameter η introduced, whose model is

$$\begin{aligned} &\min_{\chi}\ \varepsilon_1 \\ &s.t.\ \left|\chi^T\mathbf{b}_0\right| - \eta\|\chi\|_2 \ge 1 \\ &\quad \left|\chi^T\mathbf{b}_s\right| + \eta\|\chi\|_2 \le \varepsilon_1, \theta_s \in \Omega_s \end{aligned} \quad (18)$$

where $\mathbf{b}_0 = \left[e^{jkx_1\sin\theta_0} \cdots e^{jkx_N\sin\theta_0}\right]^T$ is the steering vector in the main radiation direction θ_0, and $\mathbf{b}_s = \left[e^{jkx_1\sin\theta_s} \cdots e^{jkx_N\sin\theta_s}\right]^T$ is the steering vector in the sampling direction θ_s in the side-lobe area.

2)In the case of keeping χ solved at the previous step unchanged, increase α_n to reduce the error power $P_0(\theta)$.

From above we solve the pattern synthesis problem of the center frequency, and next we will focus on the pattern synthesis problem of the first sideband. At the first sideband $m = 1$, according to (10), we have

$$F_1(\theta) = \sum_n\left(w_n^*(\alpha_n+\Delta\alpha_n)\,\mathrm{sinc}\left[\pi(\alpha_n+\Delta\alpha_n)\right] \times e^{jkx_n\sin\theta - j\pi(2\beta_n+\alpha_n+2\Delta\beta_n+\Delta\alpha_n)}\right) \quad (19)$$

In the following of this part, with χ calculated, only the influence of $\Delta\beta_n$ is considered, and similarly we assume $\Delta\beta_n \overset{i.i.d.}{\sim} N\left(0, \sigma_2^2\right)$, so

$$F_1(\theta) = \sum_n w_n^*\alpha_n\mathrm{sinc}(\pi\alpha_n)\,e^{jkx_n\sin\theta - j\pi(2\beta_n+\alpha_n+2\Delta\beta_n)} \quad (20)$$

Denoting $h_n = w_n^*\alpha_n\mathrm{sinc}(\pi\alpha_n)\,e^{-j\pi(2\beta_n+\alpha_n)}$, (20) can be transformed into

$$F_1(\theta) = \sum_n h_n e^{jkx_n\sin\theta} + \sum_n\left(e^{-j2\pi\Delta\beta_n} - 1\right)h_n e^{jkx_n\sin\theta} \quad (21)$$

Further writing (21) in vector form, we have

$$F_1(\theta) = \mathbf{h}^T\mathbf{b}_\theta + \mathbf{h}^T\mathbf{b}'_\Delta \quad (22)$$

For the convenience of analysis, we define $\mathbf{h} = \left[h_1 \cdots h_n\right]^T$ and

$$b'_\Delta = \left[\left(e^{-j2\pi\Delta\beta_1} - 1\right)e^{jkx_1\sin\theta} \cdots \left(e^{-j2\pi\Delta\beta_N} - 1\right)e^{jkx_N\sin\theta}\right]^T$$

which is the term related to the error. The steering vector is also represented by $\mathbf{b}_\theta = \left[e^{jkx_1\sin\theta} \cdots e^{jkx_N\sin\theta}\right]^T$. Analyzing the error term $\mathbf{b}'_\Delta$, we have

$$\begin{aligned} \mathcal{E}\left(\mathbf{b}'_\Delta\right) &= \left(e^{-2\pi^2\sigma_2^2} - 1\right)\mathbf{b}_\theta \\ \mathcal{D}\left(\mathbf{b}'_\Delta\right) &= \left(1 - e^{-4\pi^2\sigma_2^2}\right)\mathbf{I}_{N\times N} \\ \mathcal{E}\left(\left\|\mathbf{b}'_\Delta\right\|_2^2\right) &= N\left(1 - e^{-4\pi^2\sigma_2^2}\right) \end{aligned} \quad (23)$$

where $\mathbf{I}_{N\times N}$ represents identity matrix.

It can be seen from (22) that the error term in $F_1(\theta)$ is $\mathbf{h}^T\mathbf{b}'_\Delta$, whose statistical average power is

$$P_1(\theta) = \mathcal{E}\left\{\left(\mathbf{h}^T\mathbf{b}'_\Delta\right)\left(\mathbf{h}^T\mathbf{b}'_\Delta\right)^H\right\} = \left(1 - e^{-4\pi^2\sigma_2^2}\right)\mathbf{h}^H\mathbf{h} \quad (24)$$

So when the parametric vector $\mathbf{h}$ is unchanged, the greater the variance σ_2^2 is, the greater the error power $P_1(\theta)$ is. Furthermore

$$\mathbf{h}^H\mathbf{h} = \sum_n\left|\chi_n^2\right|\mathrm{sinc}^2(\pi\alpha_n) \quad (25)$$

So we get

$$P_1(\theta) = \left(1 - e^{-4\pi^2\sigma_2^2}\right)\sum_n\left|\chi_n^2\right|\mathrm{sinc}^2(\pi\alpha_n) \quad (26)$$

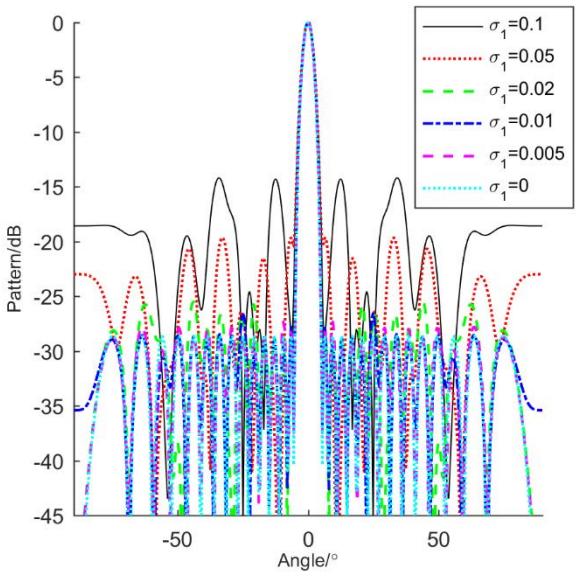

FIGURE 3. The influence of different duration time errors on the center frequency pattern.

With σ_2^2 and χ_n unchanged, increasing the normalized duration time of array elements can reduce the error power.

Defining a new parametric vector $\mathbf{g} = \left[g_1 \cdots g_n \right]^T$ of which the $n-th$ entry is $g_n = \text{sinc}\,(\pi\alpha_n)\, e^{-j\pi(2\beta_n+\alpha_n)}$, so $\mathbf{h} = \chi \cdot \mathbf{g}$ holds. The robust pattern synthesis problem at the first sideband can be solved through the following optimization model.

$$\begin{aligned} &\max_{\mathbf{g}} \mu_1 \\ &s.t.\ |(\chi \cdot \mathbf{g})\, \mathbf{b}_1| \geq \mu_1 \\ &\quad |(\chi \cdot \mathbf{g})\, \mathbf{b}_s| \leq \varepsilon_2, \theta_s \in \Omega_s \\ &\quad |\mathbf{g}| \leq \mu_2 \end{aligned} \tag{27}$$

where χ is a known parametric vector solved by (18), $\mathbf{b}_1 = \left[e^{jkx_1 \sin\theta_1} \ \cdots \ e^{jkx_N \sin\theta_1} \right]^T$ is the steering vector of the main radiation direction of the first sideband, and $\mathbf{g}$ is the parametric vector we need to obtain. μ_1 is the maximum radiation intensity at the radiation direction of the first sideband, and ε_2 is the side-lobe constraint parameter. μ_2 is the control parameter, and the smaller μ_2 is, the smaller sinc $(\pi\alpha_n)$ and error power are obtained, so that the side-lobe performance of the first sideband can be better.

Denoting the amplitude and phase of g_n are a_{gn} and φ_{gn}, respectively, after obtaining $\mathbf{g}$ by the convex optimization method, we can calculate α_n and β_n through the following relationship

$$\begin{cases} \alpha_n = \frac{1}{\pi}\text{sinc}^{-1}\left(a_{gn}\right) \\ \beta_n = -\frac{1}{2\pi}\left(\varphi_{gn} + \text{sinc}^{-1}\left(a_{gn}\right) + 2\pi p\right) \end{cases} \tag{28}$$

In the above formula, it's necessary to take an appropriate integer p to make $0 \leq \alpha_n, \beta_n \leq 1$, and the complex excitation coefficient of each element can be obtained by $w_n^* = \chi_n / \alpha_n$.

TABLE 1. 500 simulation results of different σ_1 (unit: dB).

σ_1	0.1	0.05	0.02	0.01	0.005	**0**
$Mean\{F_0(\theta_0)\}$	-0.03	-0.03	-0.01	0	0	**0**
$Var\{F_0(\theta_0)\}$	0.95	0.19	0.03	0.01	0	**0**
$Mean\{PSLL\}$	**-13.80**	**-19.00**	**-23.95**	**-26.06**	**-27.28**	**-28.64**
$Var\{PSLL\}$	2.45	2.42	1.39	0.53	0.18	**0**
$Max\{PSLL\}$	-9.35	-14.23	-20.03	-24.06	-25.71	**-28.64**

Note: $Mean\{\ \}$, $Var\{\ \}$ and $Max\{\ \}$ respectively represent the statistical mean, statistical variance and maximum value.

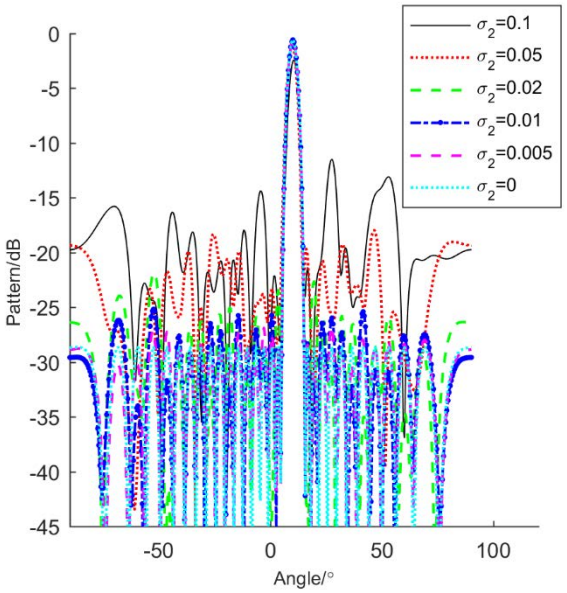

FIGURE 4. The influence of different opening time errors on the first sideband pattern.

TABLE 2. 500 simulation results of different σ_2 (unit: dB).

σ_2	0.1	0.05	0.02	0.01	0.005	**0**
$Mean\{F_1(\theta_1)\}$	**-2.17**	**-0.98**	**-0.63**	**-0.58**	**-0.56**	**-0.56**
$Var\{F_1(\theta_1)\}$	0.23	0.01	0	0	0	**0**
$Mean\{PSLL\}$	**-13.35**	**-17.90**	**-22.97**	**-25.35**	**-26.86**	**-28.64**
$Var\{PSLL\}$	2.06	1.52	0.95	0.43	0.17	**0**
$Max\{PSLL\}$	-9.42	-14.29	-19.98	-23.40	-25.57	**-28.64**

IV. SIMULATION

In order to verify the performance of the proposed algorithm, we design a set of simulation experiments, and at the same time provide corresponding figures and tables from four aspects. The configuration of the experiment is listed as follows. The time-modulated array has $N = 30$ elements and the interval of each element is $d = 0.5\lambda$. The pattern synthesis parameters are listed below: 1)The radiation direction of the center frequency is $\theta_0 = 0°$. 2)The radiation direction of the first sideband is $\theta_1 = 10°$. 3)the beam width of the center frequency and first sideband are all 10°.

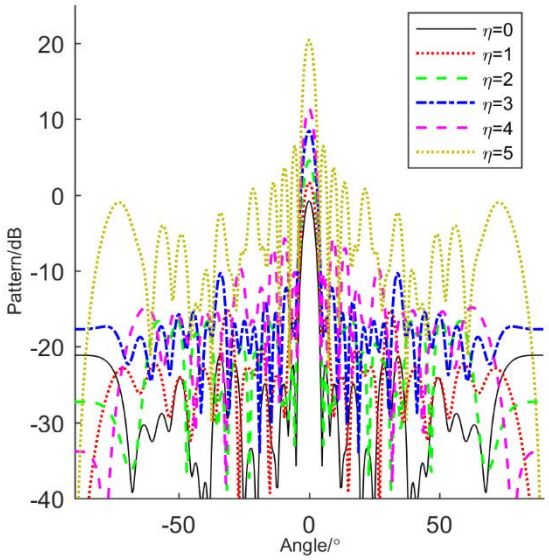

FIGURE 5. The influence of different η on the center frequency pattern with $\sigma_1 = 0.05$.

TABLE 3. 500 simulation results of statistical average of normalized side-lobe levels under different parameters(unit: dB).

η \ σ_1	0.1	0.05	0.02	0.01	0.005	0
0	-13.89	**-19.03**	-23.94	-26.02	-27.31	-28.64
1	-13.75	**-19.08**	-23.91	-26.00	-27.26	-28.64
2	-13.89	**-19.03**	-23.88	-26.06	-27.28	-28.64
3	**-13.49**	**-18.23**	**-21.97**	**-23.15**	**-23.70**	**-24.28**
4	-13.03	**-16.99**	-19.14	-19.68	-19.89	-20.09
5	-12.24	**-14.59**	-14.80	-14.87	-14.88	-14.88

A. COMPREHENSIVE ANALYSIS OF DUAL-BAND PATTERN UNDER TIME-MODULATION PARAMETER ERRORS

This section describes the effect of time-modulation parameter errors on the dual-band pattern. It can be seen from (12) that the radiation intensity of the center frequency is only related to the normalized duration time error $\Delta\alpha_n$ and has nothing to do with the normalized opening time error $\Delta\beta_n$.

Fig 3 shows the influence of different normalized duration time errors on the center frequency pattern. It can be seen that due to the normalized duration time error $\Delta\alpha_n$, the side-lobe performance deteriorates, and as the variance of the error σ_1^2 increases, the rise of the side-lobe level is more obvious.

Table 1 shows the statistical data of the 500 repeated simulation results. It can be seen that the average value of the PSLL has risen from the error-free -28.64dB to -13.80dB, -19.00dB, -23.95dB, -26.06dB, and -27.28dB, respectively, which is consistent with the above conclusion.

As for the first-order sideband, it can be seen from (20) that when χ is determined, the radiation intensity is affected by the normalized opening time error $\Delta\beta_n$.

Fig 4 shows the influence of different normalized opening time errors on the first sideband pattern. As the variance of the error σ_2^2 increases, the side-lobe level rises more obviously.

TABLE 4. 500 simulation results of statistical root of variance of normalized side-lobe levels under different parameters (unit: dB).

η \ σ_1	0.1	0.05	0.02	0.01	0.005	0
0	3.22	**2.34**	1.19	0.47	0.18	0
1	2.78	**2.19**	1.33	0.49	0.18	0
2	3.24	**2.32**	1.35	0.54	0.17	0
3	**3.29**	**2.39**	**0.87**	**0.33**	**0.10**	**0**
4	2.68	**1.95**	0.67	0.21	0.06	0
5	2.10	**1.67**	0.41	0.09	0.03	0

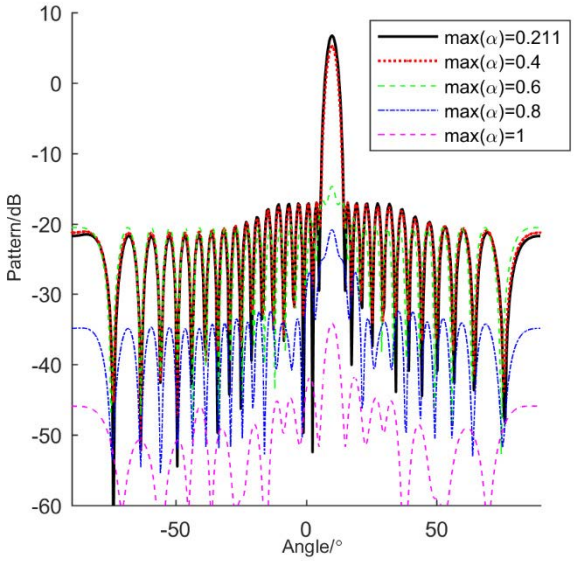

FIGURE 6. First sideband pattern with different maximum duration time.

Table 2 shows the statistical results of 500 experiments. It can be seen from Table 2 that with the increase of σ_2, the maximum radiation intensity of the main-lobe is decreasing, while the mean of PSLL is increasing.

B. ANALYSIS OF ANTI-ERROR ROBUST PATTERN SYNTHESIS OF CENTER FREQUENCY

In this section, we will study the influence of the parameter η on the performance of the center frequency pattern according to (18).

Fig 5 shows the influence of different η on the center frequency pattern with $\sigma_1 = 0.05$. It can be seen that as η increases, the maximum of the radiation intensity increases, and the PSLL also increases. In order to further obtain the statistical performance of the algorithm we proposed, we performed 500 repeated simulations on multiple sets of parameters, and the results are shown in Table 3 and Table 4.

Table 3 shows the statistical average of the normalized side-lobe level in 500 random experiments under different σ_1 conditions when η takes a specific value, from which we can see: 1)When keeping η unchanged, such as the row of $\eta = 3$, the normalized side-lobe level increases as the parameter σ_1 increases. 2)When keeping σ_1 unchanged, for example, in the column of $\sigma_1 = 0.05$, from a statistical point of view, the

TABLE 5. 500 simulation results of different max (α_n) (unit: dB).

$\max(\alpha_n)$	0.21	0.4	0.6	0.8	1
$Mean\{NPSLL\}$	-21.91	-23.05	-23.84	-24.17	-24.25
$\sqrt{Var\{NPSLL\}}$	0.98	0.37	0.06	0.0044	0.0002

Note: NPSLL means normalized-PSLL.

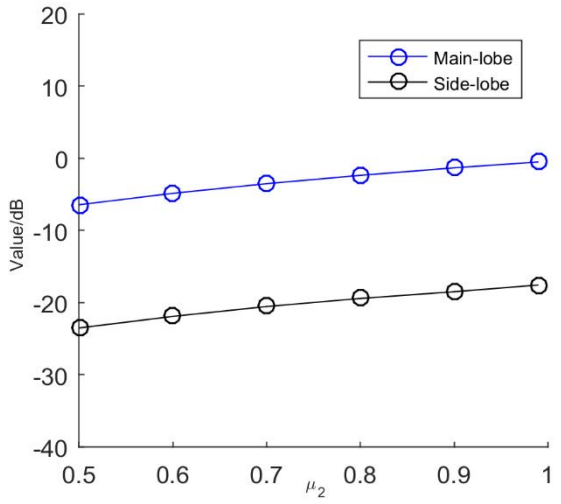

FIGURE 7. The influence of μ_2 on the maximum radiation intensity and peak side-lobe level.

normalized side-lobe level increases with the increase of η, which shows that setting the upper bound parameter η cannot improve the deterioration of side-lobe level.

Table 4 shows the statistical root of variance of the normalized side-lobe level, that is, the deviation degree of the normalized side-lobe level in 500 random experiments under the different σ_1 conditions when η takes the specific values, respectively. From this table we can see clearly: 1)When keeping η unchanged, such as the row of $\eta = 3$, the degree of deviation increases with the increase of σ_1. 2)When keeping σ_1 unchanged, such as the column of $\sigma_1 = 0.05$, the degree of deviation decreases as η increases, which shows that setting the upper bound parameter η can reduce the side-lobe deterioration range.

Combining the conclusion of the Table 3 and Table 4, it can be seen that although the upper bound parameter η cannot lighten the uplift of the side-lobe caused by the error, it can reduce the dynamic range of its fluctuation, which is exactly the meaning of the so-called 'robustness' in the algorithm.

Furthermore, in order to make the side-lobe performance better, we can reduce the statistical average and the statistical root of variance of the normalized side-lobe level by increasing $\max(\alpha_n)$. Table 5 shows the statistical results of 500 repeated simulations of the center frequency pattern when α_n is increased proportionally under the setting of $\eta = 3, \sigma_1 = 0.02$.

However, increasing α_n proportionally will affect the radiation characteristics of the first sideband. As shown in Fig 6,

TABLE 6. The statistical average value of the maximum radiation intensity of the first sideband in 500 simulations under different parameters(unit: dB).

μ_2 \ σ_2	0.1	0.05	0.02	0.01	0.005	0
0.5	-7.65	**-6.43**	-6.09	-6.04	-6.02	-6.02
0.6	-6.10	**-4.85**	-4.50	-4.45	-4.44	-4.44
0.7	-4.70	**-3.52**	-3.16	-3.11	-3.10	-3.10
0.8	-3.57	**-2.35**	-2.00	-1.95	-1.94	-1.94
0.9	-2.52	**-1.33**	-0.98	-0.93	-0.92	-0.92
0.99	-1.72	**-0.50**	-0.15	-0.10	-0.09	-0.09

TABLE 7. The statistical average value of peak side-lobe level of first sideband in 500 simulations under different parameters (unit: dB).

μ_2 \ σ_2	0.1	0.05	0.02	0.01	0.005	0
0.5	-18.85	**-23.46**	-28.49	-30.84	-31.77	-31.85
0.6	-17.25	**-21.94**	-26.96	-29.25	-30.12	-30.27
0.7	-15.95	**-20.58**	-25.58	-27.90	-28.85	-28.93
0.8	-14.70	**-19.45**	-24.41	-26.77	-27.65	-27.77
0.9	-13.69	**-18.33**	-23.39	-25.73	-26.63	-26.74
0.99	-12.92	**-17.51**	-22.55	-24.92	-25.78	-25.92

the first sideband need to be further optimized for robust pattern synthesis of dual frequency bands.

C. ANALYSIS OF ANTI-ERROR ROBUST PATTERN SYNTHESIS OF FIRST SIDEBAND

It can be seen from the previous part that increasing α_n will worsen the radiation characteristics of the first sideband. So it is necessary to adjust the parameter μ_2, according to (27), to further control the value of α_n to improve the radiation characteristics of the first sideband $f_0 + f_r$. This part shows the influence of μ_2 on the first sideband pattern.

Fig 7 shows that as μ_2 takes the value 0.5, 0.6, 0.7, 0.8, 0.9 and 0.99 in turn with $\sigma_2 = 0.05$, the statistical average value of the maximum radiation intensity of the main-lobe and PSLL are increasing. Furthermore, in order to obtain the statistical results of the maximum radiation intensity and PSLL of the first sideband under different parameters, we perform 500 repeated experiments on multiple sets of parameters. The results are shown in Table 6 and Table 7.

Table 6 and Table 7 respectively give the statistical average values of the maximum first sideband radiation intensity and PSLL in 500 repeated experiments when the specific values of the parameter μ_2 are taken respectively under the different values of σ_2, from which we can find : 1)When keeping the parameter μ_2 unchanged with the increase of σ_2, the maximum radiation intensity decreases along with the increase of the PSLL.

2)When keeping σ_2 unchanged, as the parameter μ_2 increases, the maximum radiation intensity increases, and the PSLL also increases.

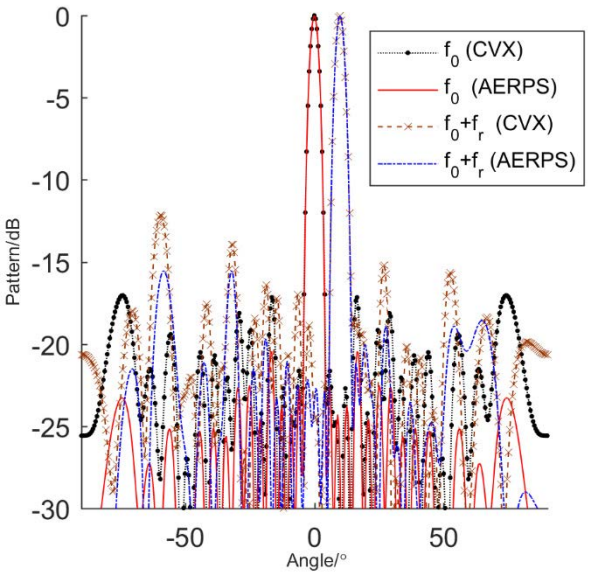

FIGURE 8. Results of the maximum radiation intensity and peak side-lobe level of the two algorithms.

TABLE 8. Comparison of 500 simulation results of two algorithms (unit: dB).

	CVX		AERPS	
	f_0	f_0+f_r	f_0	f_0+f_r
$Mean\{\max(F(\theta))\}$	-0.02	-1.18	7.27	3.57
$Var\{\max(F(\theta))\}$	**0.18**	**0.17**	**0.03**	**0.02**
$Mean\{PSLL\}$	-19.08	-15.93	-14.48	-12.32
$Var\{PSLL\}$	2.02	1.91	0.79	1.61
$Mean\{NPSLL\}$	**-19.06**	**-14.75**	**-21.75**	**-15.88**
$Var\{NPSLL\}$	**2.02**	1.99	**0.79**	1.84

Note: $F(\theta)$ here means $F_0(\theta_0)$ and $F_1(\theta_1)$ corresponding to the different frequency band.

It can be concluded that adjusting parameter μ_2 can control the performance of the main-lobe and side-lobe under the error condition, but the performance improvement of the main-lobe and side-lobe are often contradictory. Therefore, it's necessary to select the appropriate μ_2 based on the prior knowledge of the error variance σ_2^2 to achieve a better trade-off between the main-lobe and side-lobe performance.

D. ANALYSIS OF ANTI-ERROR ROBUST PATTERN SYNTHESIS OF DUAL-BAND

Combining the analysis results of above parts, we will take a specific setting of the parameters $\eta = 3, \mu_2 = 0.7$ to verify the performance of the algorithm we proposed(another setting of the parameters can also reflect the performance of the algorithm to vary degrees), and compare with the algorithm of $\eta = 0, \mu_2 = 1$ (that is, the CVX algorithm without processing).

Fig 8 shows the dual-band normalized pattern under two algorithms. It can be seen that the proposed algorithm can make the side-lobe performance better. In order to further give the performance of the algorithm in a statistical sense, we have done 500 repeated experiments, and the results are shown in Table 8.

Table 8 shows the performance comparison between the unprocessed CVX algorithm and AERPS algorithm under the specific setting of $\sigma_1 = 0.05, \sigma_2 = 0.05$. It can be seen that the radiation intensity of the proposed AERPS algorithm in the direction of the center frequency $\theta_0 = 0°$and first sideband $\theta_1 = 10°$ all increases, and the statistical variance is significantly reduced.

The statistical variance of the maximum radiation intensity at the center frequency is reduced from 0.18dB to 0.03dB, and the statistical variance of the maximum first sideband radiation intensity is reduced from 0.17dB to 0.02dB, which embodies the significant improvement of the robustness of the pattern synthesis.

V. CONCLUSION

Aiming at the dual-band time-modulated linear array pattern synthesis model with errors, this paper proposes an AERPS algorithm, which can reduce the side-lobe lift caused by errors and improve the robustness of the pattern synthesis. Our basic idea is to divide the model into two sub-models and further solve the revised model step by step through making reasonable assumptions about the distribution of the time-modulation parameter errors. We first perform convex optimization solution for the center frequency band, and then perform convex optimization solution for the first sideband after obtaining the intermediate parametric variables, and finally obtain the complex excitation coefficient, opening time and duration time of each element. This paper shows the effectiveness and robustness of the algorithm through the simulation results of 30-element linear array. It can be seen from the results that the algorithm proposed in this paper can reduce the normalized side-lobe level in a statistical sense, and reduce the dynamic range of the normalized side-lobe level.

REFERENCES

[1] B. Appasani, R. Pelluri, and N. Gupta, "Detection and correction of errors in linear antenna arrays," *Int. J. Numer. Modelling, Electron. Netw., Devices Fields*, vol. 31, no. 5, p. e2453, Sep. 2018.
[2] Z. Amir and B. A. Arand, "GA-based approach to phase compensation of large phased array antennas," *J. Syst. Eng. Electron.*, vol. 29, no. 4, pp. 723–730, Aug. 2018.
[3] X. Huang, K. Hao, L. U. Mingdi, R. Fan, and Q. Wan, "A self-calibration method for gain-phase errors of airborne antenna array using multiple measurements," *Telecommun. Eng.*, vol. 58, no. 1, pp. 13–17, 2018.
[4] Y. Xie, S. Liu, R. Ding, and P. Li, "Phased-array surface monitoring method based on compensation correction technique," in *Proc. IOP Conf. Mater. Sci. Eng.*, vol. 585, no. 1, Jul. 2019, Art. no. 012112.
[5] F. Zhang, W. Fan, Z. Wang, Y. Zhang, and G. F. Pedersen, "Improved over-the-air phased array calibration based on measured complex array signals," *IEEE Antennas Wireless Propag. Lett.*, vol. 18, no. 6, pp. 1174–1178, Jun. 2019.
[6] Z. Dai, E. Su, and H. Gu, "A gain and phase autocalibration approach for large-scale planar antenna arrays," *IEEE Commun. Lett.*, vol. 25, no. 5, pp. 1645–1649, May 2020.

[7] K. Wang, J. Yi, F. Cheng, Y. Rao, and X. Wan, "Array errors and antenna element patterns calibration based on uniform circular array," *IEEE Antennas Wireless Propag. Lett.*, vol. 20, no. 6, pp. 1063–1067, Jun. 2021.
[8] P. Rocca, N. Anselmi, A. Benoni, and A. Massa, "Probabilistic interval analysis for the analytic prediction of the pattern tolerance distribution in linear phased arrays with random excitation errors," *IEEE Trans. Antennas Propag.*, vol. 68, no. 12, pp. 7866–7878, Dec. 2020.
[9] G. He, X. Gao, and R. Zhang, "Impact analysis and calibration methods of excitation errors for phased array antennas," *IEEE Access*, vol. 9, pp. 59010–59026, 2021.
[10] S. Lou, W. Wang, H. Bao, N. Hu, G. Ge, X. Hu, S. Qian, and C. Ge, "A compensation method for deformed array antennas considering mutual coupling effect," *IEEE Antennas Wireless Propag. Lett.*, vol. 17, no. 10, pp. 1900–1904, Oct. 2018.
[11] D.-G. Yoo, D.-H. Kim, H.-S. Kim, and K.-W. Lee, "A study on waveguide slotted active phased array radar target information error compensation technique," *J. Korea Inst. Mil. Sci. Technol.*, vol. 22, no. 1, pp. 11–19, 2019.
[12] X. Ye, W.-T. Li, and W. Du, "An equivalent method of position error caused by the array antenna deformation," *Prog. Electromagn. Res. Lett.*, vol. 74, pp. 53–60, 2018.
[13] E. Sippel, M. Lipka, J. Geib, M. Hehn, and M. Vossiek, "*In-situ* calibration of antenna arrays within wireless locating systems," *IEEE Trans. Antennas Propag.*, vol. 68, no. 4, pp. 2832–2841, Apr. 2020.
[14] C. Wang, Y. Wang, X. Yang, W. Gao, C. Jiang, L. Wang, Y. Zhang, and M. Wang, "Effect of randomness in element position on performance of communication array antennas in Internet of Things," *Wireless Commun. Mobile Comput.*, vol. 2018, pp. 1–8, Mar. 2018.
[15] G. Sa, Z. Liu, C. Qiu, and J. Tan, "A hybrid tolerance design method for the active phased-array antenna," *Appl. Sci.*, vol. 10, no. 4, p. 1435, Feb. 2020.
[16] C. Wang, S. Yuan, W. Gao, C. Jiang, Y. Yan, Y. Zheng, Z. Wang, M. Wang, and X. Song, "A prior knowledge-based algorithm for robust design of array antennas with interval excitation and position uncertainties," *IEEE Trans. Antennas Propag.*, vol. 69, no. 3, pp. 1355–1368, Mar. 2021.
[17] X. Zhang, G. Liao, Z. Yang, and S. Li, "A position error calibration algorithm for conformal arrays," Nat. Lab. Radar Signal Process., Xidian Univ., Xi'an, China, Tech. Rep., 2021, doi: 10.1049/icp.2021.0774.
[18] B. Zhou, H. Gao, and S. Wen, "Distributed coherent radar baseline selection and calibration error analysis," *Syst. Eng. Electron.*, vol. 40, no. 11, pp. 2438–2443, 2018.
[19] H. Frid, J. Malmström, and B. L. G. Jonsson, "Determining direction-of-arrival accuracy for installed antennas by postprocessing of far-field data," *Radio Sci.*, vol. 54, no. 12, pp. 1204–1221, Dec. 2019.
[20] F. Guo, Z. Liu, W. Hu, and J. Tan, "Gain prediction and compensation for subarray antenna with assembling errors based on improved XGBoost and transfer learning," *IET Microw., Antennas Propag.*, vol. 14, no. 6, pp. 551–558, May 2020.
[21] R. Zhang, Y. Wu, Z. Bian, and W. Sheng, "Sequential phase feeding algorithm with minimal beam pointing error for centrosymmetric planar array antenna," *Int. J. RF Microw. Comput.-Aided Eng.*, vol. 30, no. 8, p. e22241, Aug. 2020.
[22] S. Lee and H.-J. Song, "Accurate statistical model of radiation patterns in analog beamforming including random error, quantization error, and mutual coupling," *IEEE Trans. Antennas Propag.*, vol. 69, no. 7, pp. 3886–3898, Jul. 2021.
[23] O. Yurtsev, N. Naumovich, and A. Yubko, "Effect of time intervals random errors on time-modulated antenna parameters," in *Proc. 9th Int. Conf. Antenna Theory Techn.*, Sep. 2013, pp. 187–189.
[24] M. Amjadian and M. Fakharzadeh, "Error analysis for time modulated arrays," in *Proc. IEEE Int. Symp. Antennas Propag. USNC/URSI Nat. Radio Sci. Meeting*, Jul. 2017, pp. 493–494.

YUANJIN TIAN received the B.S. degree in information engineering from the Nanjing University of Aeronautics and Astronautics (NUAA), in 2020, where he is currently pursuing the M.S. degree in information and communication engineering with the College of Electronic and Information Engineering.

His research interest includes array signal processing.

JING TAN received the M.S. degree in signal and information processing from the Nanjing University of Aeronautics and Astronautics (NUAA), Nanjing, China, in 2006, where she is currently pursuing the Ph.D. degree.

She is currently an Associate Professor with the Department of Information Engineering, Nanhang Jincheng College, China. Her research interest includes the study of antenna array signal processing.

YANWEI ZHANG received the B.S. degree in information engineering from the Nanjing University of Aeronautics and Astronautics (NUAA), in 2020, where he is currently pursuing the M.S. degree in information and communication engineering with the College of Electronic and Information Engineering.

His research interest includes array signal processing.

KE WANG received the B.S. degree in communication engineering from Jiangxi Normal University, in 2021. She is currently pursuing the M.S. degree with the College of Electronic and Information Engineering, NUAA.

Her current interest includes array signal processing.

XIAO DONG was born in Henan, China. She received the B.S. degree from the North China University of Water Resources and Electric Power, Zhengzhou, China, in 2021. She is currently pursuing the M.S. degree with the Nanjing University of Aeronautics and Astronautics.

Her current research interests include array signal processing and array theory and technology.

HAILIN LI received the Ph.D. degree in signal and information processing from the Nanjing University of Aeronautics and Astronautics (NUAA), Nanjing, China, in 2013.

He is currently an Associate Professor with the College of Electronic and Information Engineering, NUAA. His research interests include digital signal processors, conformal array, and array signal processing.